Part I
Chapter 3

Determination of the Intrinsic Bulk and Surface Plasmon Intensity of XPS Spectra of Magnesium

M. Kurth, P.C.J. Graat, E.J. Mittemeijer

Abstract

Separation of intrinsic and extrinsic intensity contributions to plasmon peaks in X-ray photoelectron spectra of free-electron like metals (Me) such as Be, Na, Mg, Al and semiconductors as Si and Ge, necessary for the accurate determination of the thickness of overlayers in the range of a few nanometers, and their composition, is difficult because of their more or less coincident energies. The intrinsic bulk and surface plasmon contributions to Me 2p spectra can be determined separately from the intensities of the metallic and oxidic main peak as obtained from a series of spectra recorded from the non-oxidised metal and the oxidised metal with different oxide-film thicknesses. In the present work, this method was applied to XPS Mg 2p spectra. It was shown that the method is very sensitive to deviations in the measured data, and therefore a careful error analysis is required, which has been developed in this work. Furthermore, an alternative method based on the same theory was proposed. This method yielded values of 0.17 and 0.06 for the intrinsic bulk and surface plasmon contributions to the Mg 2p spectrum relative to the Mg 2p main peak for a detection angle of 45°. It was demonstrated that the values obtained for the intrinsic bulk and surface excitation contributions determined according to both methods depend on the oxide-thickness range investigated. This observation indicates that commonly applied simplifying assumptions for the oxidation behaviour of Mg, like a layer-by-layer growth mechanism and/or the development of a homogeneous oxide with bulk MgO properties, as for composition and band gap values, do not hold. The pronounced effect of neglect of the intrinsic plasmon intensity contributions on the thickness values determined for MgO films on Mg was shown.

Keywords: plasmons, magnesium, intrinsic intensity, oxidation, XPS.

3.1. Introduction

In free-electron like metals with only s and p electron orbitals, like Be, Na, Mg, and Al, collective oscillations of the conduction electrons, the so-called plasmons, are relatively pronounced. The frequency ω_p of these oscillations is different for the bulk and the surface of the material.

For free-electron like metals coupling of the localised positively charged core hole (*intrinsic* energy transfer) and the photoelectrons travelling through the material (*extrinsic* energy transfer), both created in the photoelectron emission process, with the 'gas' of free electrons causes plasmon excitations and consequently, in the (X-ray) photoelectron spectrum a plasmon fine structure occurs characterised by the energy shifts $\hbar\omega_{pb}$ or $\hbar\omega_{ps}$, for bulk plasmon (BP) and surface plasmon (SP) excitations, respectively. This leads to additional peaks at the higher binding energy side of the (metallic) main peaks of core levels in the XPS spectra. The distances on the energy scale between the plasmon peaks and the main peak equal multiples of $\hbar\omega_{pb}$ and $\hbar\omega_{ps}$. The probability of excitation for plasmons with energies equal to a multiple of $\hbar\omega_{pb}$ (or $\hbar\omega_{ps}$) is small, leading to a decaying intensity for such 'higher order' plasmon peaks.

Intrinsic plasmon excitation is caused by the coupling of the positive core holes, created by the ejection of core electrons from their orbitals, with the collective electron oscillation of the conduction electron gas [53] *simultaneously* with the photoemission process [72] *at the location* of the initial photon – electron interaction. As a result the photoelectron is ejected with less energy ($\hbar\omega_{pb}$ or $\hbar\omega_{ps}$ (or multiples of this energies), depending on the place of interaction, i.e. the bulk or surface region), than it would have had if the coupling had not occurred. Photoelectrons that stem from intrinsic plasmon excitations belong to the intrinsic (primary) electron emission spectrum together with the main peak and its asymmetric tail, which is caused by an intrinsic process too, namely the reduction of the kinetic energy of the photoemitted electrons due to scattering of the conduction electrons by the positive core hole [53].

Apart from *intrinsic* plasmon generation, *extrinsic* plasmon generation can occur as well. An *extrinsic* plasmon energy loss process [53,55,58,72] occurs by the coupling of the electric field of the photoelectron on its way through the solid with that of the free electrons in the solid. The photoelectron thereby looses the energy $\hbar\omega_{pb}$ or $\hbar\omega_{ps}$ (or multiples of this energy), depending on whether the interaction takes place in the bulk or at the surface of the sample. This process happens *after and away* from the location of the initial photoemission

process. All photoelectrons which experienced extrinsic energy loss processes, i.e. including the extrinsic plasmon excitations, belong in an XPS spectrum to the background of inelastically scattered electrons (secondary spectrum), to be distinguished from the intrinsic (primary) electron spectrum.

Now, for the determination of the thickness of a thin (a few nanometers) homogeneous layer on a metal substrate from an XPS spectrum, the *total intrinsic* (metallic) intensity of the spectrum must be taken into account. The normally used procedure of assessing only the intensity of the main peak in the spectrum will inevitably lead to false results, either overestimating or underestimating the overlayer thickness (depending on the equation used for determination of the thickness, see Section 3.2.1). These errors can easily be dramatic, as shown in Fig. 3.1.

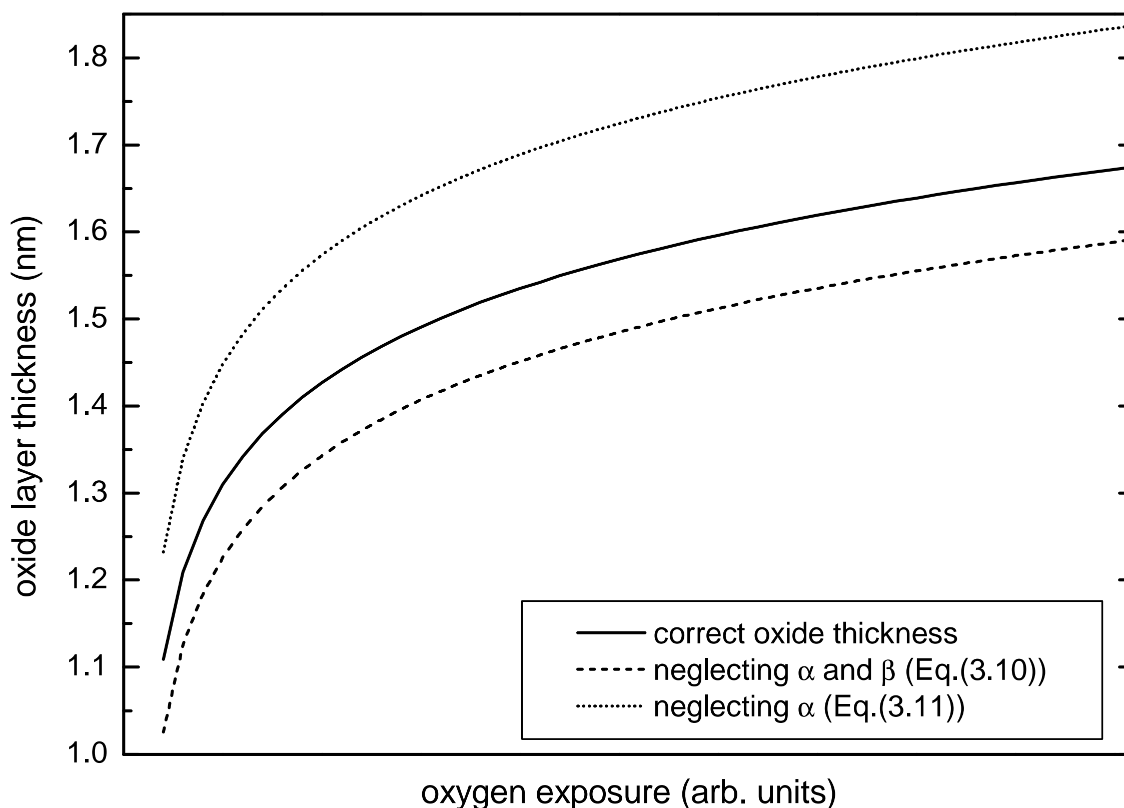

Figure 3.1: Hypothetical results of oxide layer thicknesses determined from Eqs. (3.10) and (3.11) ignoring intrinsic plasmon contributions, as compared to the true layer thickness. Here, $\alpha = 0.15$ and $\beta = 0.05$ have been used.

Hence, for correct determination of the thickness of layers on free-electron like metals it is imperative that the total primary (zero loss) intensity is determined and thus the intrinsic and extrinsic plasmon contributions have to be separated. Because both the intrinsic and extrinsic plasmon excitations require (about) the same amount of energy, their corresponding peaks

(practically) coincide in an XPS spectrum, which complicates their separation severely. Only in a few papers the determination of the intrinsic bulk plasmon excitation probability (in Mg [53] or other free electron like metals [55,72]) has been striven for, either by experimental or by theoretical analysis; the reported data differ considerably. Data of intrinsic surface plasmon excitation probabilities lack almost totally and to our knowledge the intrinsic surface plasmon contribution to XPS spectra of Mg has not been reported before.

Recently, for the first time, a method has been presented to determine separately the intensity contributions of intrinsic bulk and surface plasmon excitations to the primary, 'zero loss', Al 2p spectrum [56]. In that method only the metallic main peak region of a reference spectrum of a clean metal sample and the metallic and oxidic main peak regions of spectra of a series of oxidised samples of the same metal with different oxide-layer thicknesses are used. In the present paper the applicability of this method has been investigated by application to XPS data recorded from (oxidised) magnesium. It followed that an elaborate data treatment is required to reduce the error to an acceptable level. Against this background an alternative method, based on the same theoretical background and using the same spectra, has been presented as well. Both methods have been compared.

3.2. Theoretical background

The ratio of the intensity originating from the intrinsic plasmon excitation relative to the intensity originating from the core level excitation (i.e. the main peak plus its asymmetric tail) will be denoted α for the bulk plasmon excitation and β for the surface plasmon excitation. Then, the total intrinsic intensity, I_m^{ref}, of a photoelectron line (the primary spectrum) originating from a clean metallic sample is given by:

$$I_m^{ref} = J_m^{ref}(1+\alpha+\beta) \tag{3.1}$$

with J_m^{ref} being the integrated intensity of the main peak (including asymmetric tail) in a spectrum of the clean metal. The total intrinsic intensity, I_m, of the same photoelectron line originating from the same metal substrate covered with an (oxide) layer is given by:

$$I_m = J_m(1+\alpha) \tag{3.2}$$

with J_m being the integrated intensity of the 'metallic' main peak (including asymmetric tail) in a spectrum of the oxidised metal substrate. It thus is assumed that the surface plasmon peak (and thus β in Eq. (3.2)) vanishes completely after coverage of the metal with more than one monolayer of oxygen because of the chemical bonding (highly ionic in the case of Mg)

between oxygen and the metal. Thus, the electrons of the surface atoms of the metal will become localised and therefore do not participate in the free electron 'gas'. The total intrinsic intensity, I_{ox}, of the photoelectron line originating from the metal ions in the oxide layer is given by:

$$I_{ox} = J_{ox} \tag{3.3}$$

with J_{ox} being the integrated intensity of the 'oxidic' main peak in the spectrum of the oxide layer. This equation implies, that there are no *intrinsic* bulk and surface plasmon contributions due to the metal oxide (see discussion in Ref. [56]).

The intensities of a photoelectron line originating from an oxidised metal are (see for example Ref.[73]):

$$I_m = I_m^{ref} \exp\left[-\frac{d_{ox}}{\lambda_{ox}\cos\theta}\right] \tag{3.4}$$

for the metallic substrate contribution, and

$$I_{ox} = I_{ox}^{ref}\left[1-\exp\left(-\frac{d_{ox}}{\lambda_{ox}\cos\theta}\right)\right] \tag{3.5}$$

for the oxidic layer contribution to the spectrum. In Eqs. (3.4) and (3.5) λ_{ox} denotes the inelastic mean free path (IMFP) of photoelectrons travelling through the oxide film; d_{ox} is the oxide film thickness; θ is the angle between the sample normal and the detection direction and I_{ox}^{ref} is the total intrinsic intensity of the pure oxide. I_m^{ref} and I_{ox}^{ref} are related by:

$$\frac{I_{ox}^{ref}}{I_m^{ref}} = \frac{C_{ox}\lambda_{ox}}{C_m\lambda_m} \tag{3.6}$$

with C_{ox} and C_m being the volume densities of the metal atoms in the oxide and in the metal, respectively and λ_m being the IMFP of photoelectrons travelling through the metal substrate From Eqs. (3.4), (3.5) and (3.6) it follows:

$$\frac{I_{ox}}{I_m} = \frac{C_{ox}\lambda_{ox}}{C_m\lambda_m}\left[\exp\left(\frac{d_{ox}}{\lambda_{ox}\cos\theta}\right)-1\right] \tag{3.7}$$

Inserting Eqs. (3.1), (3.2), (3.3) and (3.4) into Eq. (3.7) finally yields [56]:

$$\frac{J_m^{ref}}{J_m} = \frac{1+\alpha}{1+\alpha+\beta} + \frac{K}{1+\alpha+\beta}\frac{J_{ox}}{J_m} \tag{3.8}$$

with $K = C_m\lambda_m / C_{ox}\lambda_{ox}$. Hence if a series of oxidised metal substrates with different oxide-layer thicknesses is available, plotting of J_m^{ref} / J_m versus J_{ox} / J_m should yield a straight line

with the intercept $a=(1+\alpha)/(1+\alpha+\beta)$ and the slope $b=K/(1+\alpha+\beta)$. From the slope and intercept of that straight line the values for the intrinsic bulk plasmon contribution α and the intrinsic surface plasmon contribution β can be calculated separately:

$$\alpha=\frac{a}{b}K-1 \qquad \text{and} \qquad \beta=\frac{1-a}{b}K \tag{3.9}$$

Note, that all of the intensity values in Eq. (3.8) are *main* peak intensities, thereby avoiding the explicit separation of intrinsic and extrinsic plasmon intensities in each of the spectra recorded, which is the essence of this method to determine α and β.

3.2.1. Alternative method for determination of α and β

Ignoring the intensity contribution of the intrinsic bulk and surface plasmon peaks (i.e. substituting I by J in Eqs. (3.4) and (3.7)) leads to wrong oxide layer thicknesses determined from equations like (3.4) or (3.7), both applicable in the range of a few nanometers. Then, depending on which equation is used, one obtains an overestimation or an underestimation of the oxide-layer thickness. From Eq. (3.4) it follows:

$$d_{ox}=\lambda_{ox}\cos\theta\ln\left(\frac{J_m^{ref}(1+\alpha+\beta)}{J_m(1+\alpha)}\right) \tag{3.10}$$

In this case, ignoring α and β (both > 0) leads to an underestimation of the oxide-layer thickness, which is independent of the oxide-layer thickness. Thus, the relative error in the layer thickness increases with decreasing thickness. From Eq. (3.7) it follows:

$$d_{ox}=\lambda_{ox}\cos\theta\ln\left(K\frac{J_{ox}}{J_m(1+\alpha)}+1\right) \tag{3.11}$$

In this case, ignoring α and β (both > 0) leads to an overestimation of the oxide-layer thickness, which depends on thickness.

A typical evolution of the oxide-film thickness during low-temperature oxidation of metals is shown in Fig.1, together with the thickness values which would be obtained from XPS measurements according to Eqs. (3.10) and (3.11) if α and β would be neglected.

Obviously, application of the correct values for α and β in Eqs. (3.10) and (3.11) should yield equal results for the oxide layer thickness d_{ox}. Hence, minimising the difference between the results for the thickness values determined from these two equations by a fit procedure, with α and β as fit parameters provides a straightforward way to determine the correct intrinsic bulk and surface plasmon excitation probabilities.

3.3. Experimental

3.3.1. Base material and sample preparation

Polycrystalline magnesium rods with a mean grain diameter of ~ 25 µm and a purity of 99.95 wt % (supplier: Alfa, Johnson Matthey GmbH) were cut to discs of 1 to 2 mm in height and 15 mm in diameter. The samples were ground with SiC paper (1200 - 4000 ≙ 15 to 8 µm grains) and subsequently mechanically polished with diamond paste (6 µm, 3 µm and 1 µm grains) using a mix of distilled water, ethanol and liquid soap as a lubricant. To remove the mechanically distorted surface due to grinding and polishing, the samples were etched with a mixture of ethanol (98 vol. %), HCl (1.2 vol. %) and HNO_3 (0.8 vol. %) for 130 s, which made the grain boundaries just visible upon inspection with a light-optical microscope. Finally, the samples were sputter cleaned with a 3kV Ar^+ beam (raster size: at least 3 mm x 3 mm; angle of incidence: 42°) in the UHV chamber of the XPS system until survey XPS spectra (recorded in the binding energy range of 0 - 1400 eV with a pass energy of 89.45 eV and a step size of 1eV/step) showed no peaks due to elements other than Mg.

3.3.2. Oxidation experiments

After sputter cleaning in UHV, the samples were oxidised with pure oxygen (purity 99.997 vol. %) in the same UHV chamber. Oxidation was carried out mainly in series of successive oxidation experiments each followed by an XPS measurement. In one series the oxidation experiment was carried out at a certain temperature (in the range of 273 K to 436 K) and at a certain oxygen partial pressure (in the range of $1.3 \cdot 10^{-8}$ Pa to $1.3 \cdot 10^{-5}$ Pa), for different oxidation times (varying from 2 min to 120 min). The samples were heated by resistive heating of the sample holder. The temperature was measured with a Chromel/Alumel thermocouple attached ~1 mm away from the centre of the back of the sample holder and ~1 mm away from the heating spool placed at the back of the holder, too. During oxidation, the oxygen partial pressure was recorded using a Vacscan quadrupole mass spectrometer. After each oxidation experiment and subsequent XPS measurements, the sample was sputter cleaned again, until the absence of oxygen was confirmed by XPS survey spectra. Altogether 129 oxidation experiments with 6 identically prepared samples were executed under the conditions described above.

Since with this procedure only a few oxide layers which were thicker than about 1.7 nm were created, additionally two samples, prepared as described above, were oxidised at 673 K for 120 min at ~10^5 Pa oxygen partial pressure in a separate oxidation furnace, in order to

get relatively thick oxide layers. Then, these samples were brought into the XPS measurement chamber. An initial sputter treatment removed surface contamination. With successive cycles of Ar^+-sputtering and XPS-measurement, 43 additional spectra were obtained, covering the oxide-layer thickness range of 1.6 nm to 5.6 nm.

Furthermore, from one sample oxidised at 673 K for 1200 min at ~10^5 Pa oxygen partial pressure an electron-transparent cross section was prepared that was investigated with transmission electron microscopy with a 200 keV Zeiss instrument. For protection of the sample from further oxidation during the ion thinning preparation procedure, a thin Ti-sealing has been evaporated onto the oxidised Mg sample prior to the cross section preparation.

3.3.3. XPS measurements

XPS spectra were recorded in a PHI 5400 ESCA system using non-monochromatic Al Kα radiation (15 kV, 300 W). The energy scale of the hemispherical analyser was calibrated using the Ag $3d_{5/2}$ peak set at 368.3 eV. The intensity scale was corrected for the analyser transmission function as described in Ref. [74]. Furthermore, since the intensities varied in the course of time, a correction of the intensities was necessary to make all the XPS measurements comparable. This was achieved using the intensity ratio of the Mg 2p peak observed in survey XPS spectra of the sputter cleaned metal, recorded before each oxidation experiment, and the same peak observed in a survey spectrum of the reference sample of the pure metal recorded prior to a (detailed) measurement of this reference spectrum (see below). Each spectrum recorded after oxidising the sample was then corrected by multiplication of the measured intensity values by the corresponding intensity ratio.

Before carrying out each oxidation series (after sputter cleaning), the Mg 2p peak of the bare metal substrate was measured in the binding energy range from at least 44 to 84 eV. This spectrum was used as the reference spectrum of the pure metal. After each oxidation experiment both the Mg 2p peak (recorded in the range of at least 44 to 83 eV) and the O 1s peak (recorded in the range of 526 to 540 eV) were measured. Furthermore, the Mg 2p and O 1s peaks of a sputter cleaned MgO single crystal were measured. All spectra (except the survey measurements) were recorded with a constant pass energy of 17.9 eV and a step size of 0.05 eV. All measurements were performed at an angle $\theta = 45°$ between the sample normal and the detection direction. At this angle the (elliptically-shaped) analysed area was about 1.1 mm x 1.6 mm.

3.4. Data evaluation

For the determination of α and β according to both methods described in section 3.2 the main peak intensity ratios J_m^{ref} / J_m and J_{ox} / J_m have to be determined from the measured Mg 2p spectra. To this end the spectra were evaluated as follows.

First, the x-ray satellites caused by the presence of Al $K_{\alpha3}$, Al $K_{\alpha4}$, Al $K_{\alpha5}$, Al $K_{\alpha6}$ and Al K_{β} in the incident radiation were removed from all spectra, using the procedure described in Ref. [66]. Then a constant background intensity was subtracted, to account for instrumental noise and for contributions of photoelectron lines at higher kinetic energies. For this background intensity the average value of the minimum intensity value at the lower binding energy side of the main peak of the spectrum and the next 10 data points (0.5 eV) to the higher binding energy side was used. This procedure sets the intensity of the lower binding energy side of the spectrum to zero.

The intensity J_m^{ref} was obtained from the spectra of the sputter-cleaned metallic sample. To this end the background of photoelectrons that had experienced inelastic interactions (i.e. including the photoelectrons that suffered energy losses due to extrinsic plasmon excitation) was subtracted from the main peak region (electron binding energy range of 45 eV to 52 eV), applying the method of Tougaard [47,48] and using the 'universal cross section' for inelastic electron 'scattering' [57,75]. This method has been shown (for Ag, Pt and Au) to yield better results than the straight line method or the Shirley method [76]. The use of the 'universal cross section' is well suited for noble and transition metals but is actually not correct for the case of simple metals like Mg, where electron energy loss is mainly caused by extrinsic plasmon excitations [58]. However, for the small main peak region considered here the inelastic background contribution is very small (note that the (extrinsic) plasmon peak *maxima* occur at considerably higher binding energies; cf. Fig. 3.2), and the actual shape of the cross section has negligible influence on the main peak intensities resulting from this procedure.

After subtraction of the background of inelastically 'scattered' electrons in the main peak region, the intensities in the main peak region of the metallic reference sample was fitted with an asymmetric Gauss-Lorentz function [66] in the binding energy range of 45 eV to 52 eV.

This range clearly excludes the plasmon peak region (see Fig. 3.2). The fitted curve was then extended over the whole measured energy range (up to 84 eV; thereby the tail of the metallic main peak in the region of the plasmon peaks is included) and integration of the extended curve yielded J_m^{ref} (see full line shown in Fig. 3.2).

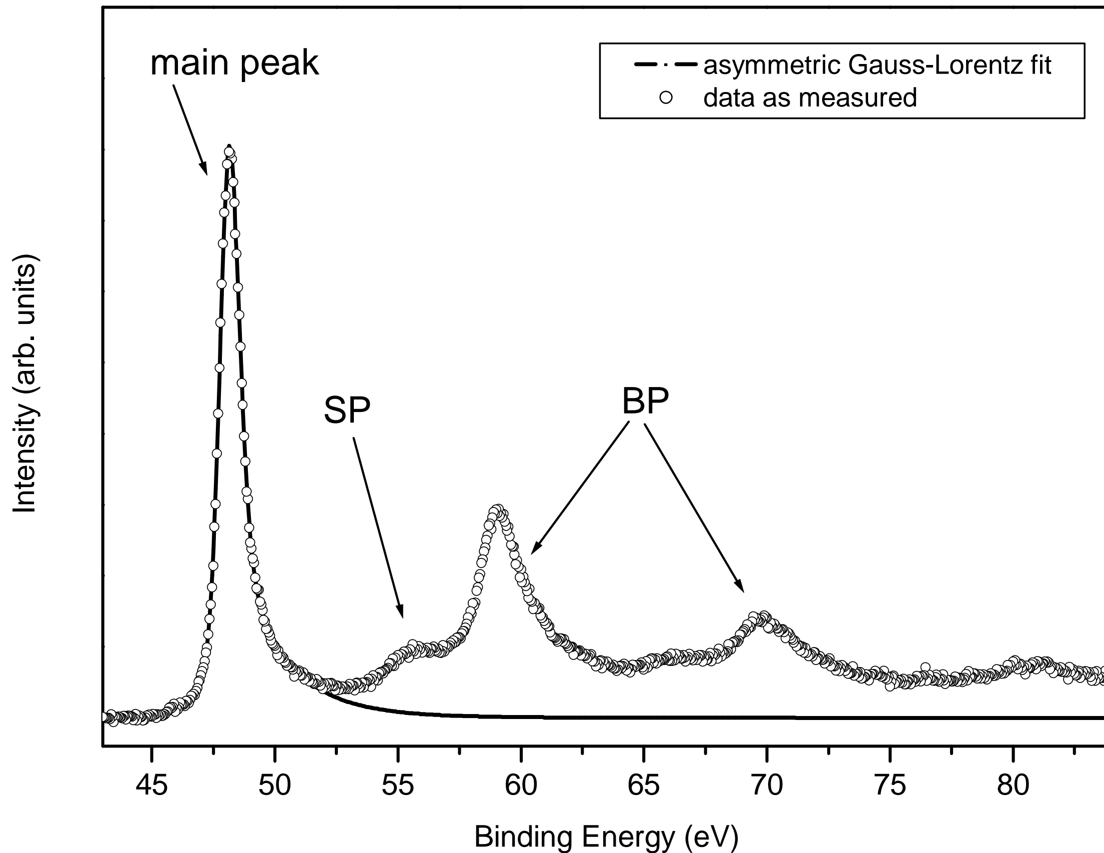

Figure 3.2: Mg 2p main peak and plasmon region as measured for sputter-cleaned Mg. An asymmetric Gauss-Lorentz function has been fitted to the main peak in the binding energy range of 45 eV to 52 eV (after background subtraction) and has been extrapolated over the whole region. The area under the fitted curve is J_m^{ref} .

The intensities J_m and J_{ox} were determined from the Mg 2p spectra recorded after oxidation. In these spectra the metallic and oxidic main peaks overlap (Fig. 3.3). To separate these contributions the asymmetric Gauss-Lorentz shape was taken for the metallic part again, using the curve parameters determined from the metallic reference spectrum. Only the peak height was varied in correspondence with an assumed thickness for a homogeneous oxide layer on the metal substrate. Additionally a small shift (maximal 0.25 eV) of the position of the metallic main peak has been allowed to account for small fluctuations on the energy scale in the case of the experiments in the UHV chamber; for the furnace oxidations a shift of maximal 0.75 eV has been allowed due to increasing charging effects with increasing oxide

thickness. For the thus calculated metallic main peak the background of inelastically 'scattered' electrons corresponding to the oxide-layer thickness considered was calculated and added to the curve, applying Tougaards' method as described in Refs. [49,50]. The resulting curve (metallic main peak plus corresponding background) was subtracted from the combined metallic and oxidic main peaks of the oxidised sample. Thus, a rest spectrum remained which was assumed to consist of only the oxidic main peak, originating from Mg in the oxide layer.

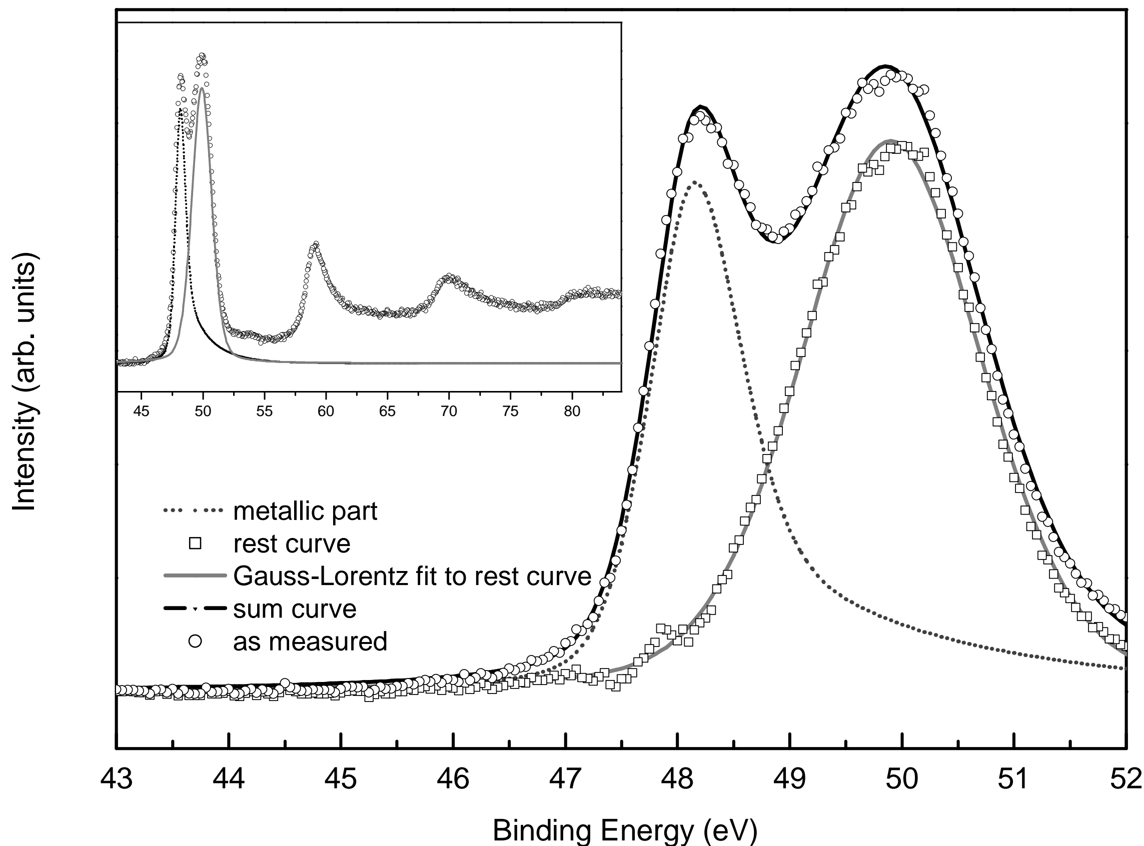

Figure 3.3: Mg 2p main peak as measured for Mg oxidised for 40min at $p_{o2} = 1.3 \cdot 10^{-5}$ Pa and T = 436 K. The main metallic and oxidic peak was fitted in the binding energy range of 45 eV to 52 eV as described in the text. The resulting curves for the metallic and oxidic contributions extrapolated to the whole region measured are shown in the inset. The areas under these curves are J_m and J_{ox} , respectively. To illustrate the very good correspondence between fit and experimental data, the sum curve of the metallic and oxidic parts is shown with addition of the respective background, and can be compared with the measured experimental data.

From this 'oxidic' rest spectrum a calculated background of inelastically 'scattered' electrons was subtracted, applying Tougaard's method. Then, a symmetric Gauss-Lorentz function was fitted to the remaining spectrum. This entire procedure was repeated for various assumed values of the oxide-layer thickness until the sum of the squared differences between the 'oxidic' rest spectrum and the fitted symmetric Gauss-Lorentz curve was minimal (minimisation was achieved by using the simplex search algorithm as implemented in Matlab [77]). A typical example of a resulting fit is shown in Fig. 3.3. Subsequently, the resulting

curves (without background) for the metallic and oxidic main peaks were extended over the whole measured energy range (up to 84 eV) and integration of the extended curves yielded J_m and J_{ox}.

The assumption of a symmetric Gaussian-Lorentzian peak shape for the oxidic part of the spectrum was validated by the measurement of the Mg 2p spectrum of the MgO single crystal, which was best fitted with such a curve (Fig. 3.4). Because a peak shift of about 7 eV and probably also peak broadening had occurred due to charging of the MgO single crystal sample, the curve-fit parameters obtained for the Mg 2p peak of the MgO single crystal sample could not be used directly in the fitting procedure described above for the oxidised Mg samples.

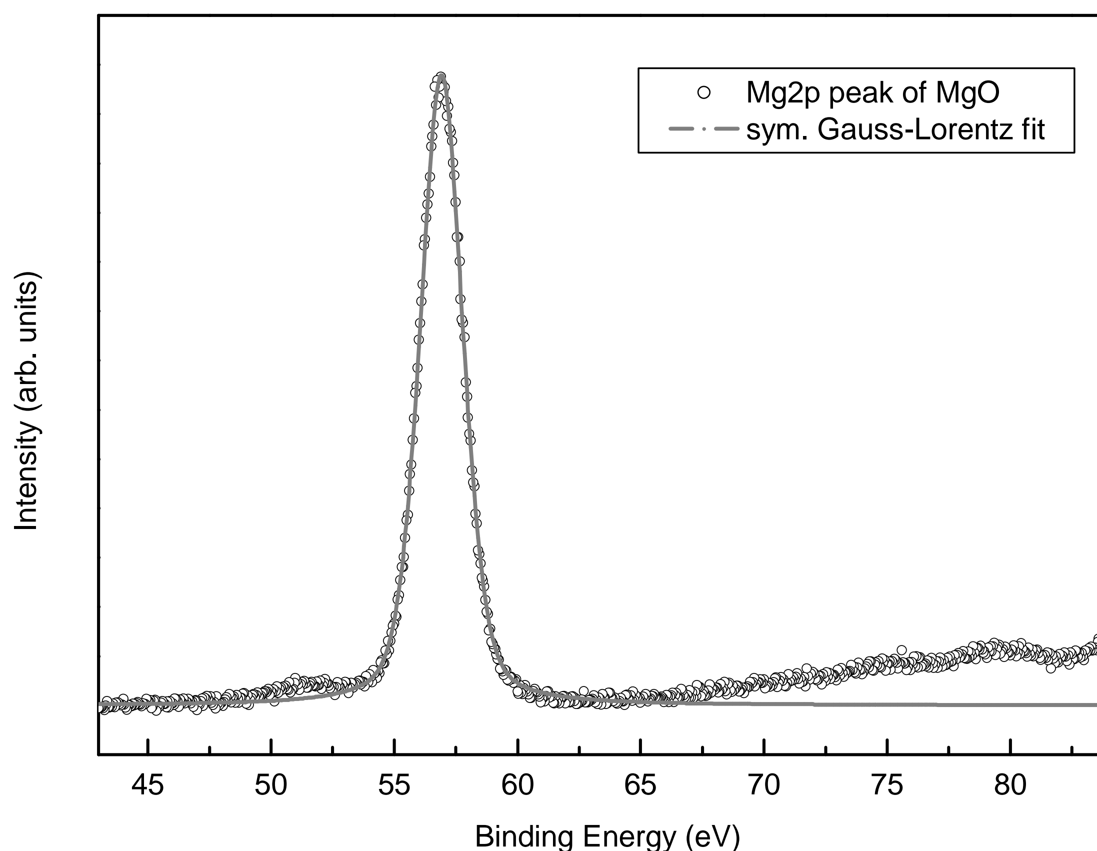

Figure 3.4: Mg 2p spectrum of a MgO single crystal. As compared to the position of the oxidic peak in the spectrum of an oxidised sample, the spectrum was shifted ~7eV to higher binding energies and probably broadened due to charging. A symmetric Gauss-Lorentz function could be fitted excellently to the main peak region. The intensity rise at the high binding energy side is due to inelastically scattered electrons which are not accounted for in the applied background elimination procedure for a homogeneous material after Tougaard.

For the calculation of the background of inelastically scattered electrons with Tougaards' method for the metallic and oxidic main peaks in the spectrum of the oxidised samples the universal cross section for electron energy loss was used. As was noted above for

the sputter cleaned metallic samples the shape of this cross section is not correct for the present case, but in view of the low background in the energy range considered for fitting, a deficiency in the shape of the cross section has negligible influence on the resulting intensities. Furthermore, it should be noted that the value of the oxide-layer thickness that results from the fitting procedure is not correct, because up to this stage, the substantial intrinsic plasmon contribution has still been ignored. This causes also a slightly wrongly calculated background *in the region of the main peaks*, but for the same reason as indicated for the cross section this has negligible influence on the resulting intensities.

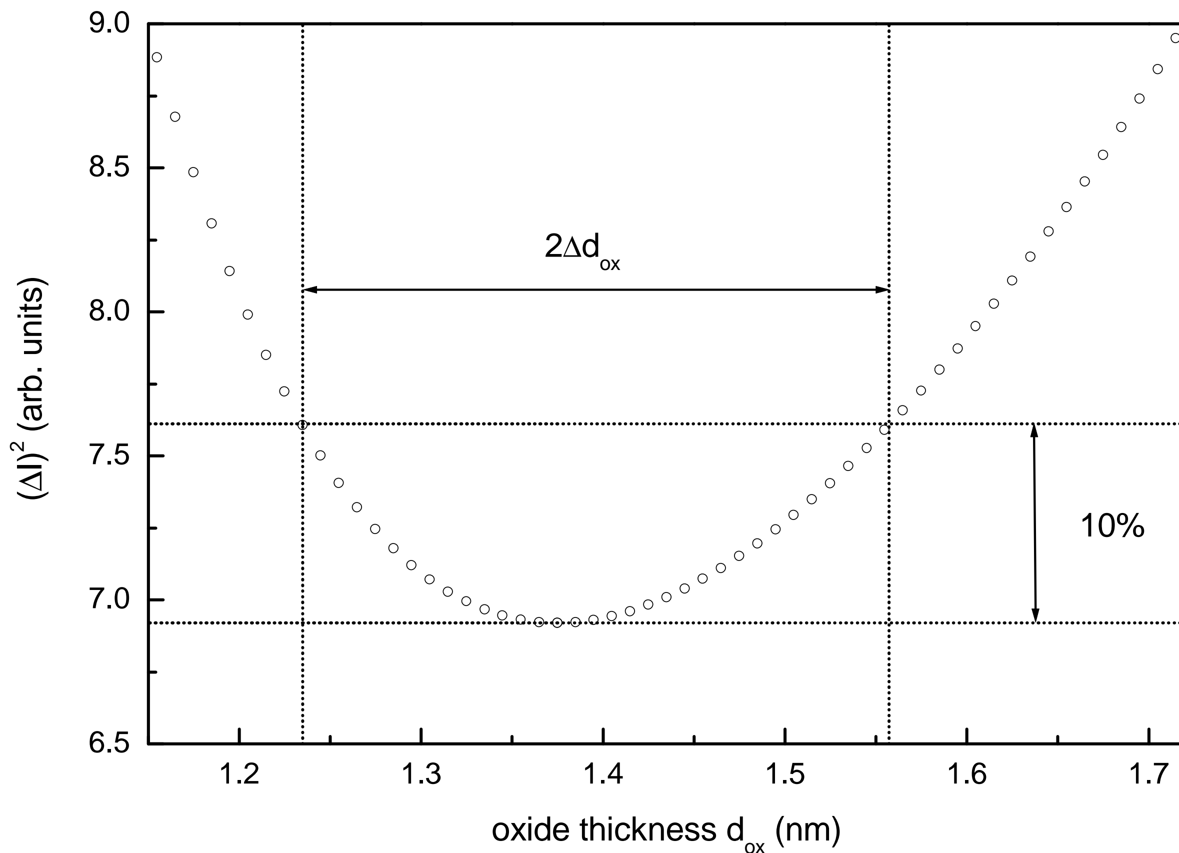

Figure 3.5: Example of sum of squared intensity differences, $(\Delta I)^2$, between oxidic 'rest' spectrum and fitted symmetric Gauss-Lorentz function versus oxide thickness, d_{ox}. The minimum of the curve equals the best fit result. The oxide thickness values leading to 10% deviation in $(\Delta I)^2$ were used for error calculation.

To be able to calculate the statistical errors of the values to be determined for the intrinsic bulk and surface plasmon contributions, α and β, the errors of the intensity determinations described above should be considered. Recognising the data evaluation procedures discussed above, it can be assumed that J_m and J_{ox} are the principal sources of error and that the error in J_m^{ref} can be neglected. To get an error estimate for J_m and J_{ox} the

sum of the squared differences between the oxidic rest spectrum and the symmetric Gauss-Lorentz function fitted to it (see above) was calculated for a range of oxide-layer thickness values around the best-fit thickness value. Then the upper and lower limits of oxide-thickness values were chosen, which correspond to a maximum deviation of the sum of the squared difference values of 10 % relative to the best-fit value (Fig. 3.5). The value of 10 % was chosen arbitrarily but the result of the goodness-of-fit test strengthened this choice, indicating rather an overestimation than an underestimation of the error (see Section 3.5).

From the values for J_{ox} and J_m corresponding to the upper and lower limits of the oxide-layer thickness the upper and lower limits of the ratio J_{ox}/J_m followed. The average difference between these limiting values of J_{ox}/J_m and the best-fit value of J_{ox}/J_m was taken as the standard deviation, $\sigma(J_{ox}/J_m)$ for each data point separately.

The standard deviation of J_m^{ref} / J_m was calculated from the average difference, ΔJ_m, between the limiting values of J_m (see above) and the best-fit value of J_m according to error propagation, i.e. $\sigma(J_m^{ref} / J_m) = J_m^{ref} / J_m^2 \, \Delta J_m$.

3.5. Results and Discussion

Results of the method based on Eq.(3.8)

Plotting J_m^{ref} / J_m versus J_{ox} / J_m for all the experimental data (Fig. 3.6) exhibits a linear behaviour as predicted by Eq. (3.8). A straight line was fitted to the data (least squares fit), assuming errors in both co-ordinate values of the data points by minimising the chi-square merit function (Ref. [78], chapter 15.3):

$$\chi^2(a,b) = \sum_{i=1}^{N} \frac{(y_i - a - bx_i)^2}{\sigma_{yi}^2 + b^2 \sigma_{xi}^2} \qquad (3.12)$$

where a and b are the intercept and slope of the straight line, respectively, N is the number of data points, x_i and y_i are the co-ordinates (J_{ox} / J_m and J_m^{ref} / J_m) of the ith data point, and σ_{xi} and σ_{yi} are the standard deviations of the ith data point, which were taken as $\sigma(J_{ox}/J_m)$ and $\sigma(J_m^{ref} / J_m)$, respectively (see end of section 3.4). The resulting values for slope and intercept and their standard deviations are: intercept a = 0.9365 ± 0.0135; slope b = 0.8521 ± 0.0167. Then, using Eq. (3.9), the following results for the intrinsic bulk plasmon excitation probability α and the intrinsic surface plasmon excitation probability β were obtained: α = 0.0519 ± 0.0369 and β = 0.0713 ± 0.0171 ($\alpha + \beta$ = 0.1232 ± 0.0407). The uncertainties in α

and β were calculated assuming only errors in slope and intercept and neglecting errors in atom densities and IMFPs.

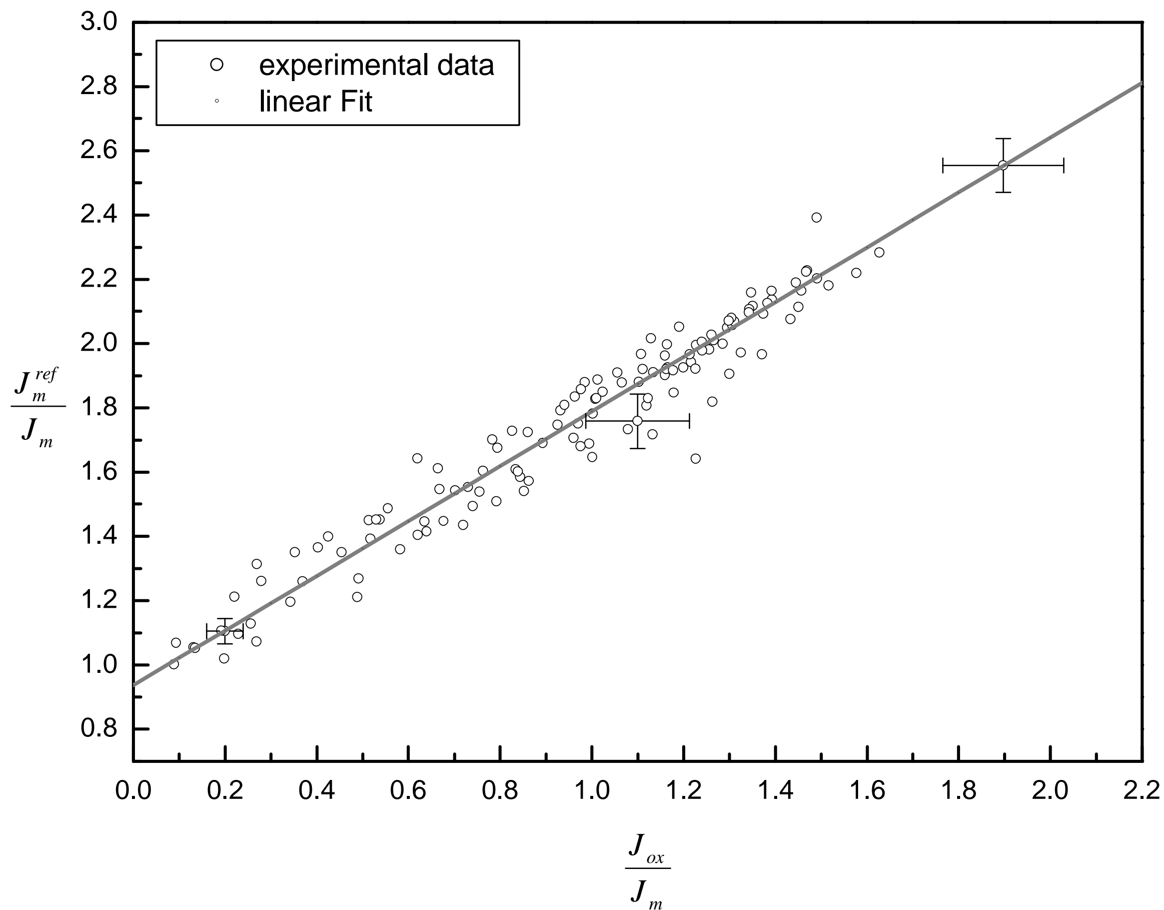

Figure 3.6: Plot of J_m^{ref} / J_m versus J_{ox} / J_m (cf. Eq. (3.8)). A straight line was fitted to the data, considering errors in both co-ordinates. Typical error bars are shown for three data points in the low, mid and high range of the plot.

For the calculation of K in Eq. (3.9) the following values were used: C_m = 71.45 mol/dm^3, which has been obtained from crystallographic unit cell parameters reported in Ref. [79], and C_{ox} = 107.98 mol/dm^3, which is the mean value obtained by evaluation of the oxidic Mg 2p main peak and the O 1s peak for all spectra recorded from the oxidised specimen [74]. This evaluation yielded a mean Mg:O ratio of 2.14. The values for C_{ox} and the Mg:O ratio given here differ significantly from the theoretical values for stoichiometric MgO with an atom density C_{ox} of 88.824 mol/dm^3 and a Mg:O ratio of 1.0 (for discussion, see Ref. [74]). The IMFPs were calculated according to Ref. [65] resulting in λ_m = 3.43 nm and λ_{ox} = 2.37 nm. For the calculation of λ_{ox} the mean value of the experimental Mg:O ratios given above was used, too.

A goodness-of-fit test (calculated as described in Ref. [78], chapt. 15 and 6) is carried out using the so-called incomplete gamma function which yields a probability Q indicating the reliability of the fit procedure, i.e. the reliability of the χ^2 determined with Eq. (3.12). The results gained here are Q = 0.9627 and χ^2 = 100.09. The value of Q indicates that the fit is good, with probably a slight overestimation of the measurement errors (see following discussion). If Q ($0 < Q < 1$) takes a very small (but non zero) value for a particular data set, then the discrepancies between the fit and the data are unlikely to be chance fluctuations. In that case it is very probable that (i) either the model is wrong, or (ii) the measurement errors are underestimated or (iii) the measurement errors are non-normal distributed. A Q value larger than ~ 0.1 indicates a believable fit [78]. If the probability Q is very large, i.e. near to 1, as in our case, it is very likely that the measurement error has been overestimated; then the value of χ^2 will become uncertain although the model can be correct. Since a non-normal distribution of measurement errors cannot produce Q values near 1 the present measurement errors are probably normally distributed. Another rule of thumb is that $\chi^2 \approx \nu$ for a χ^2 pertaining to a moderately good fit, where ν is the number of degrees of freedom which equals the number of data (129 in our case) minus the number of independent fit parameters, (2 in our case: the slope and the intercept). Thus, in the present case χ^2 should equal 127. The value obtained here is smaller (~100 vs. 127), which is likely to be due to the overestimation of the measurement errors (see above).

Note, that despite of the careful statistical analysis presented above, the results for α and β gained with this method are not very likely to be true, indicated e.g. by the relatively small value of α or $\alpha + \beta$ as compared to literature values (see discussion below) and the result that $\alpha < \beta$. One of the main reasons for this is probably the use of a constant *K,* which is doubtful since the composition of the oxide and thus the IMFPs of electrons in the oxide changes with ongoing oxidation (Ref. [74]).

Results of the method based on Eqs. (3.10) and (3.11)

The squared difference Δd_{ox}^2 between the d_{ox} values obtained with Eq. (3.10) and (3.11) were minimised, with α and β as fit parameters, using the simplex search algorithm as implemented in Matlab. In applying this new method, the constant K is calculated individually for every data point separately, i.e. instead of using mean values for C_{ox} and λ_{ox} (see above), the individual values for both quantities have been used. The result of this fit is shown in Fig. 3.7, where the thickness data as determined from Eqs. (3.10) and (3.11) with $\alpha = 0$ and $\beta = 0$ can

be compared with the thickness data as obtained from Eqs. (3.10) and (3.11) using the values for α and β as determined by fitting as described. The scattering of the data decreases with increasing oxide thickness. This is probably due to the very low oxidic Mg 2p intensity resulting from very thin oxide films in comparison to the metallic Mg 2p intensity. Statistical errors for α and β have been estimated by adding and subtracting the individual values for $\sigma(J_m^{ref} / J_m)$ and $\sigma(J_{ox}/J_m)$ (see end of section 3.4) to the corresponding intensity ratios for each data point. The Δd_{ox}^2 values corresponding to those limiting intensity ratios were minimised again, which resulted in an upper limit and a lower limit for both α and β (i.e. $\sigma_{\alpha+}$, $\sigma_{\alpha-}$ and $\sigma_{\beta+}$, $\sigma_{\beta-}$). The final results are: $\alpha = 0.0948 \pm 0.0017$ and $\beta = 0.0605 \pm 0.0043$ ($\alpha + \beta = 0.1553 \pm 0.0046$). Here, the errors indicated have been given as mean values, i.e. $\sigma_\alpha = (\sigma_{\alpha+} + \sigma_{\alpha-})/2$ and $\sigma_\beta = (\sigma_{\beta+} + \sigma_{\beta-})/2$. It should be recognised that $\sigma_{\alpha+} \neq \sigma_{\alpha-}$ and $\sigma_{\beta+} \neq \sigma_{\beta-}$. This is shown in Figs. 9 and 10 where the upper limit and the lower limit of both the α and β values are presented separately for the whole data set (the first data pair in both plots) as well as for reduced data sets (see below for detailed explanation).

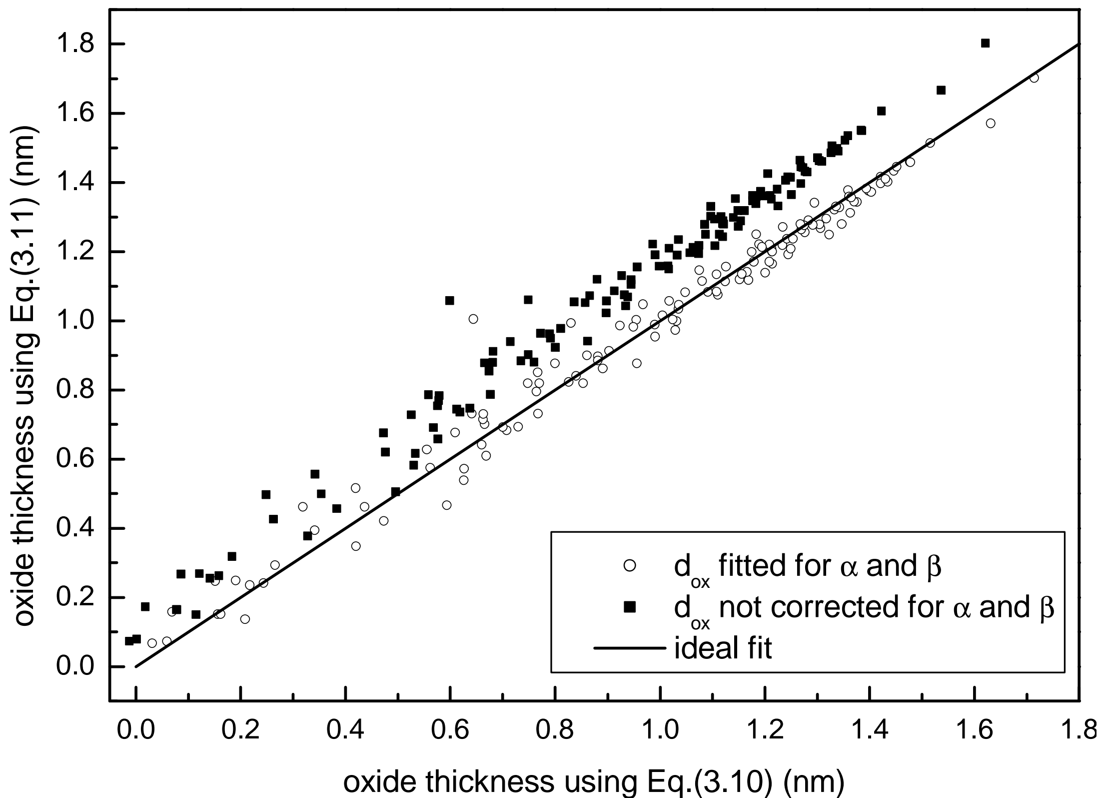

Figure 3.7: Plot of oxide thickness resulting from Eq. (3.10) vs. oxide thickness resulting from Eq. (3.11), both after fitting for α and β (alternative method). For comparison the same data not corrected for α and β are shown.

Literature data on plasmon contributions for metallic Mg

Only a few authors presented values for the intrinsic plasmon contributions in Mg metal electron emission spectra up to now. In Ref. [52] for Mg 2s only extrinsic plasmon excitations were reported. This can be due to some questionable evaluation steps in the evaluation performed in Ref. [52], like the method applied for background correction. The existence of intrinsic plasmons in Mg spectra was reported in Ref. [53]. A decreasing intrinsic plasmon creation rate (b) for increasing order of plasmon excitation (n) following a simple power law ($b_n = b^n$) was observed instead of the Poisson form ($b_n = b^n/n!$) reported in Ref. [55]. Thus, in Ref. [53], with respect to the metallic main peak intensity, for the first plasmon peak in Mg a value of 28 % was reported as well as ~ 8 % for the second plasmon peak; contributions of higher order plasmons are negligible. Thereby, in Ref. [53] a total of ~ 36 % of intrinsic plasmon intensity was reported, but any separation of surface and bulk plasmon excitations was not made. From the results reported in Ref. [55] an intrinsic intensity contribution of the plasmons of 20.9 %, with respect to the metallic main peak, can be derived. This value was obtained by consideration of only the first three bulk plasmon peaks (neglecting surface plasmon contributions) applying the Poisson form to the reported result (b = 0.19; see above). Whether the here discussed values obtained from the data in Refs. [55] and [53] are interpreted as only the bulk contribution or as bulk + surface contribution of the intrinsic plasmon contribution to the spectrum, in any case these values are larger than those obtained in this work by both methods investigated.

In another work by two of the present authors the bulk and, in contrast with the literature cited above, also surface probabilities have been determined separately, yielding α = 0. 35 and $\beta = 0.11$. Thus, $\alpha + \beta = 0.46$. This has been done by reconstruction of a metallic Mg 2p spectrum with physically realistic functions for the x-ray energy distribution, the core-level main peak, the cross sections for both bulk and surface plasmon excitations and the instrumental broadening. Thereby, possibly different electronic properties at the surface have been accounted for [80].

Note, that the most important reason for the relatively low values for α and β gained by both methods in this work compared to literature data very likely is due to the application of the band gap of bulk MgO for the calculations of the IMFP values, whereas the band gap values of the thin oxide films are probably much lower (see below for details).

Scrutinising the data and the results

The data evaluated in this work include data from oxidation experiments of very low oxygen exposures, resulting in an incomplete substrate-surface coverage with oxide, i.e. intrinsic surface plasmon excitations still contribute to the spectrum. To be certain that Eq. (3.2) applies, all data corresponding to an incomplete coverage have to be excluded from the analysis. Since the exact threshold value for the oxide-layer thickness that corresponds to the situation that no surface plasmon excitations contribute to the spectrum is unknown, it was attempted to find this threshold empirically: Data corresponding to oxide-layer thicknesses below a certain thickness value were successively removed from the original data set increasing the limit in steps of 0.1 nm. The data of these thus reduced sets were fitted following both methods as described above (based on Eq.(3.8) and on Eqs. (3.10) and (3.11), respectively) and α and β were determined for all reduced data sets. Once the threshold thickness, corresponding to a closed oxide layer, is exceeded, the values for α and β should stay constant. However, plots of α and β versus the limiting thickness value (see Fig. 3.8a and Fig. 3.9a) showed that no such constant value for α and β is reached. In particular the method based on Eq. (3.8) (Fig. 3.8a) reveals continuously changing α and β values, over the whole thickness range. Obviously, the values of α and β are correlated (see Eq. (3.9)), but even their sum does not attain a constant value (see Fig. 3.8b). On the other hand, for the new method based on Eqs. (3.10) and (3.11) $\alpha + \beta$ is nearly constant (see Fig. 3.9b).

Although experiments yielding oxide-layers of thicknesses up to ~ 1.85 nm were made, only data up to an oxide thickness limit of 1.1 nm have been considered in Fig. 3.8a,b and Fig. 3.9a,b, because the number of data points remaining upon imposing larger values for the threshold oxide-layer thickness would be too small to allow a reliable fit; unrealistic values for α and β would occur ($\beta < 0$ and/or $\alpha < \beta$). With the method based on Eq. (3.8), this instability appears to occur already at an oxide thickness limit of ~ 0.6 nm (Fig. 3.8a).

A possible origin for variable α and β values might be that the oxide-thickness range considered in this work is too small. The data cover a range for J_o/J_m between 0 to 1.6 (Fig. 3.6), which corresponds to an oxide-layer thickness range from 0 to 1.85 nm, with the upper half of this range containing twice as much data than the lower half. It was attempted to incorporate data pertaining to large layer thicknesses by making sputter-depth profiles of samples oxidised in a separate furnace at higher temperatures and pressure (see 'Experimental'). In this way oxide-layers of thicknesses in the range of 1.6 nm to 5.5 nm were obtained.

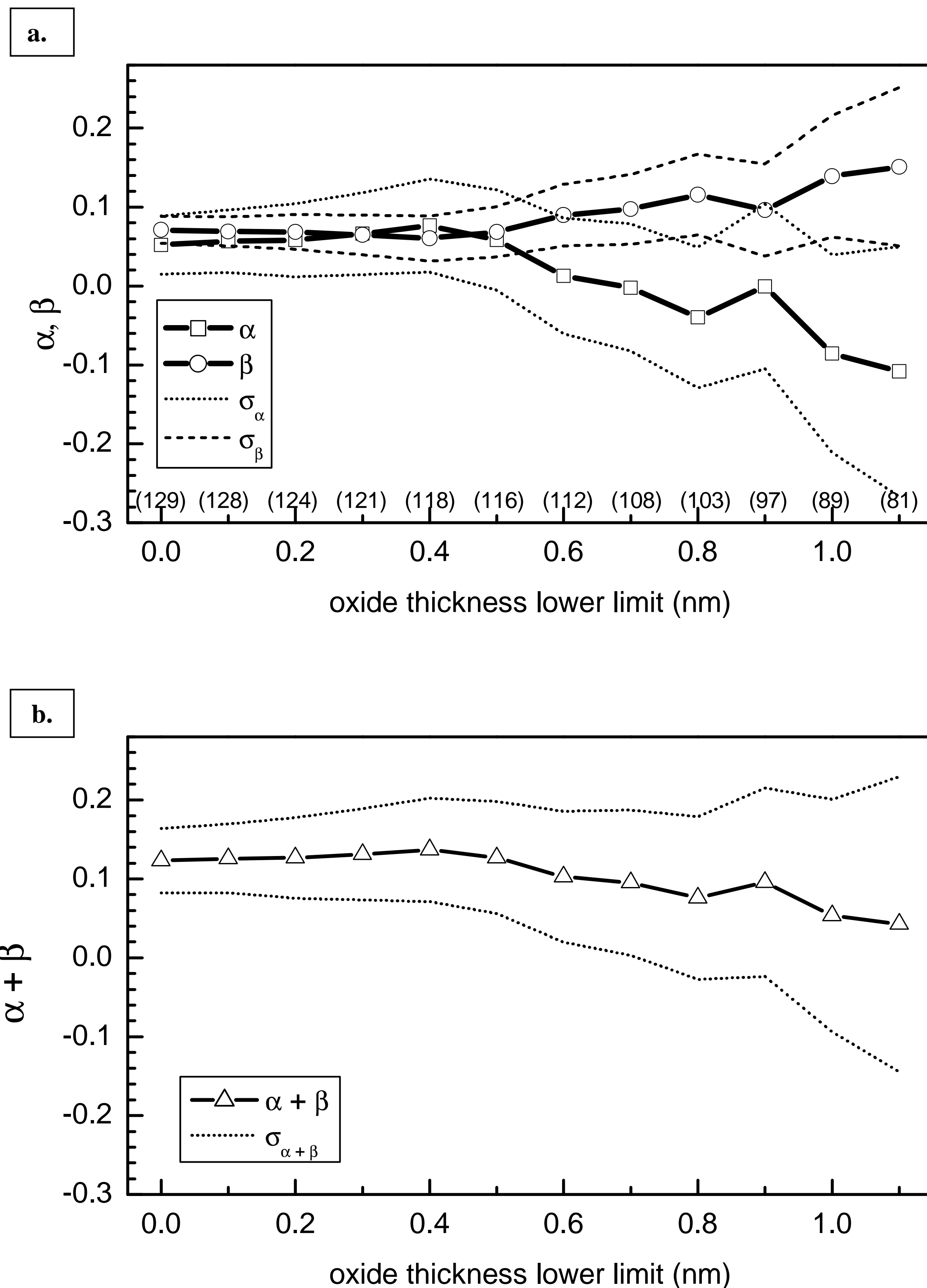

Figure 3.8: a. Results for α and β together with the corresponding error limits σ_α (dotted lines) and σ_β (dashed lines), as obtained for the method based on Eq. (3.8). Evaluations for different oxide-thickness ranges (see text) are shown. The numbers in brackets along the abscissa display the absolute number of data actually evaluated after removal of the (J_m^{ref}/J_m , J_{ox}/J_m) data of each oxidation experiment corresponding to an oxide-thickness value below a certain oxide-thickness limit. **b.** Same as in **a.** but for $\alpha + \beta$ and $\sigma_{\alpha+\beta}$ (dotted lines).

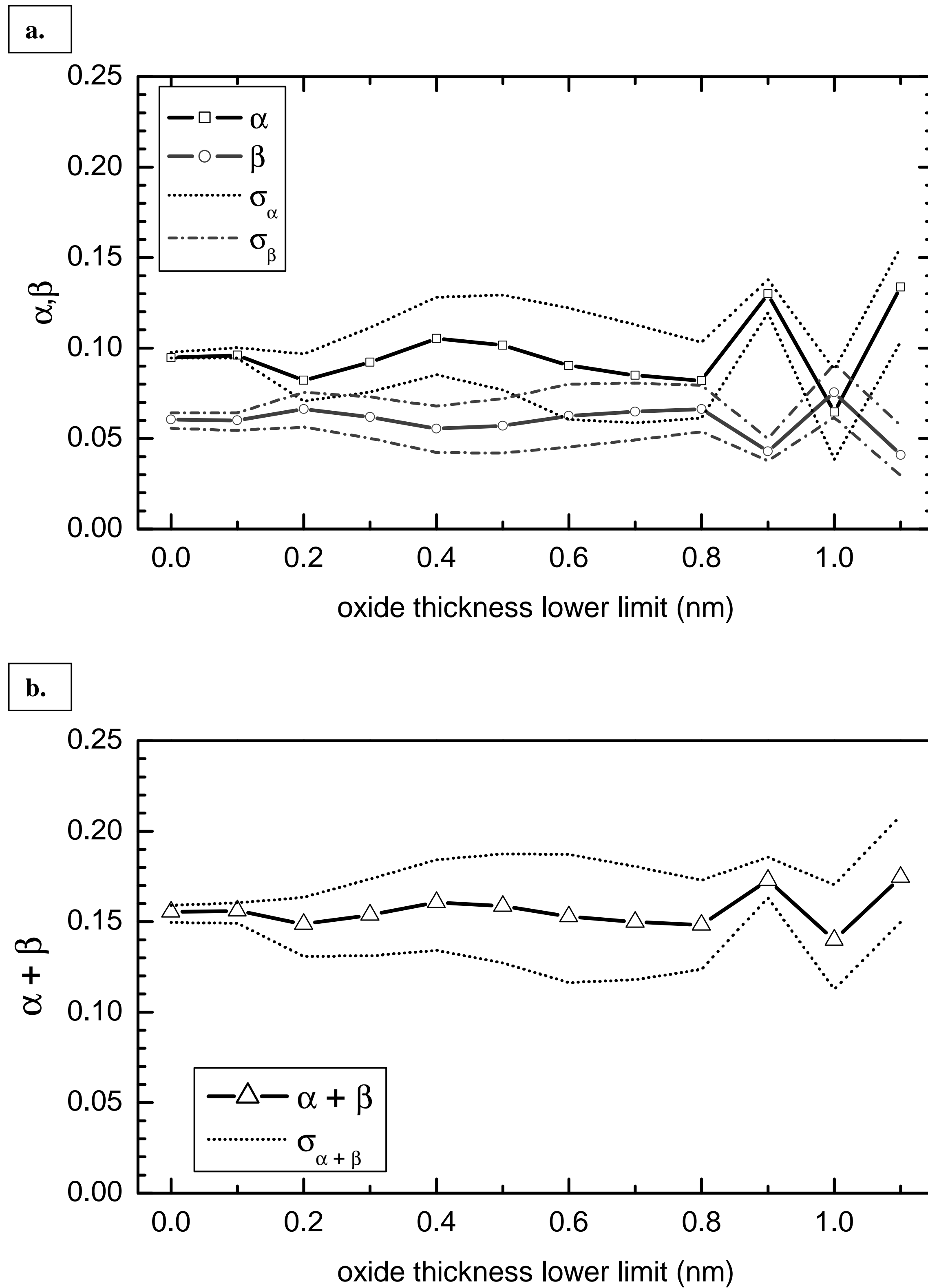

Figure 3.9: a. Results for α and β together with the corresponding error limits σ_α (dotted lines) and σ_β (dashed lines), as obtained for the alternative method (Eqs. (3.10) and (3.11)). Evaluations for different oxide thickness ranges (see text) are shown. The absolute number of data actually evaluated after removal of the (J_m^{ref} / J_m , J_{ox} / J_m) data of each oxidation experiment corresponding to an oxide-thickness value below a certain oxide thickness limit is the same as in Fig. 3.8a. **b.** Same as in **a.** but for α + β and $\sigma_{\alpha+\beta}$ (dotted lines).

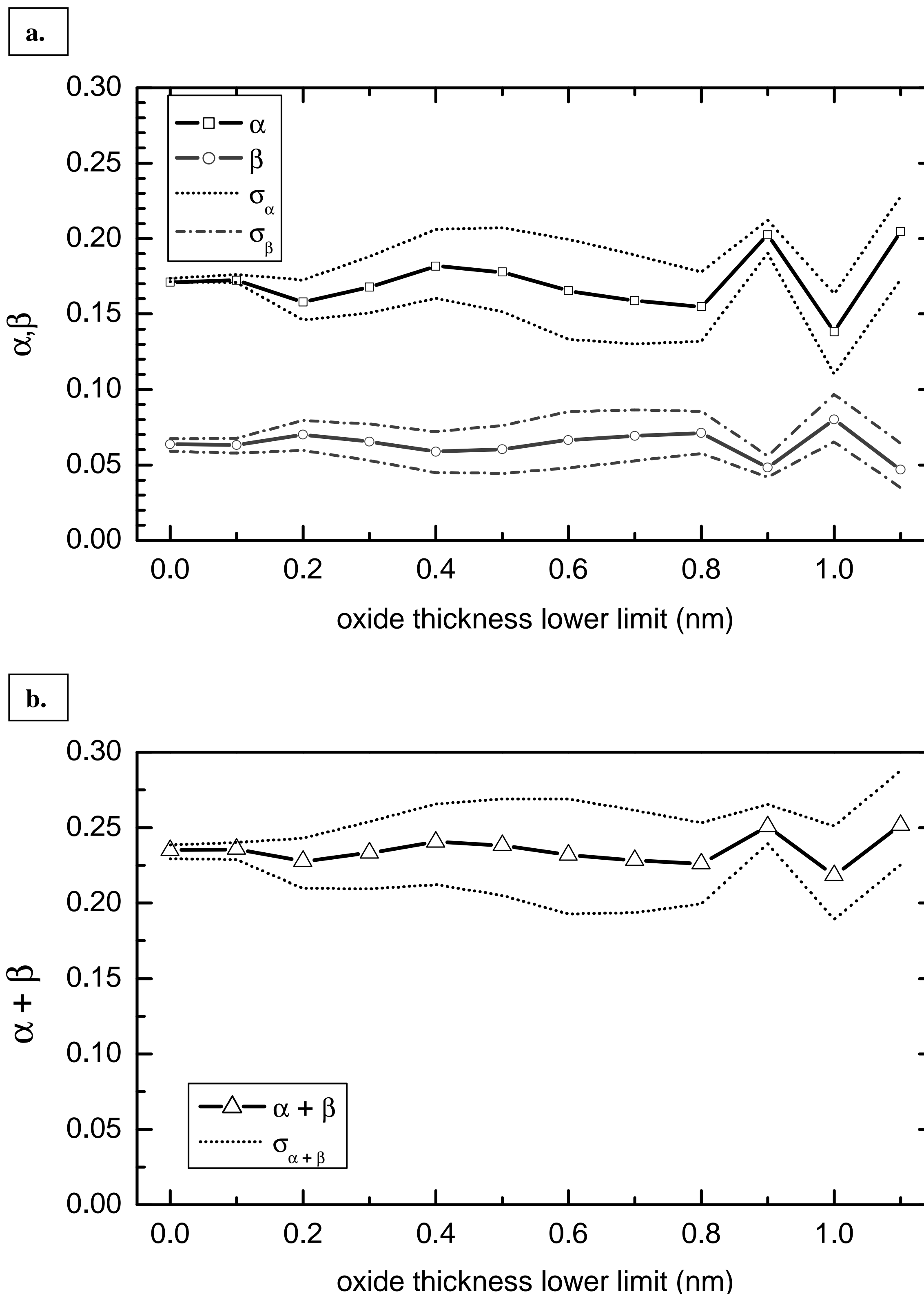

Figure 3.10: Results for α and β using a band gap energy of the oxide of 0 eV together with the corresponding error limits σ_α (dotted lines) and σ_β (dashed lines), as obtained for the alternative method (Eqs. (3.10) and (3.11)). Evaluations for different oxide thickness ranges (see text) are shown. The absolute number of data actually evaluated after removal of the $(J_m^{ref}/J_m\ ,\ J_{ox}/J_m)$ data of each oxidation experiment corresponding to an oxide-thickness value below a certain oxide thickness limit is the same as in Fig. 3.8a. **b.** Same as in **a.** but for $\alpha + \beta$ and $\sigma_{\alpha+\beta}$ (dotted lines).

Unfortunately, the composition of these oxide layers, as determined from the intensity ratio of the oxidic part of the Mg 2p peak and the O 1s peak [74], is different from the composition of the layers grown in the UHV chamber. This (slight) change in composition may be due to the thickening of the oxide or due to the different oxidation conditions. Since the composition of the oxide influences the evaluation procedure (K in Eqs. (3.8) and (3.9)), an inclusion of data of layers with different oxide composition would lead to aberrations in the results and therefore these additional data were not used in the evaluation procedure.

The evaluation procedure for the determination of the intrinsic bulk and surface plasmon excitation probabilities, α and β, following the method based on Eq. (3.8) is very sensitive to deviations in the experimental data: the small relative errors of the slope and intercept (2.0 % and 1.4 %, respectively) lead to large relative errors for α and β (71.1 % and 24.0 %, respectively; see results above). To verify whether the changing values of α and β in Fig. 3.8a,b can be explained by this statistical sensitivity or not, a plot similar to Fig. 3.8 was made, but now the increasing number of data left out for the fitting was chosen *randomly* from the original complete data set. Repetitions of this procedure yielded always similar results. A typical example is shown in Fig. 3.11. It can be seen that the scatter in the values of α and β occurring upon leaving out an increasing amount of randomly chosen data (Fig. 3.11), and as compared to the case of successively leaving out data corresponding to increased layer thickness (Fig. 3.8), is significantly smaller and shows no significant trend: especially the α-curve does not tend towards negative values like in Fig. 3.8. The results in Fig. 3.11 demonstrate that neither the trend in the (α)-values shown in Fig. 3.8 nor the extent of the scattering in the α and β values in Fig. 3.8 can have a statistical origin only.

One possibility to explain non-constant values for α and β when data corresponding to different thickness ranges are considered (Figs. 3.8a,b and 3.9a,b) could be non-uniformity of the layer thickness. Transmission electron microscopy (TEM) performed in this work for the Mg sample oxidised in a furnace at 673 K for 1200 min at 10^5 Pa oxygen partial pressure, showed an inhomogeneous oxide-layer thickness. Such an inhomogeneous layer thickness might be caused by an island growth mechanism in the initial oxidation stage [20,22,36,45].

A further possibility for α and β variation as a function of oxide-layer thickness could be a change of layer composition with thickness. Application of Eq. (3.8) requires (through the constant K) knowledge of the volume densities of the metal atoms in the oxide and in the metal; also for the calculation of the IMFPs in the metal and in the oxide, according to Ref. [65], these volume densities have to be known. From the intensities of the oxidic Mg 2p main

peak and the O1s peak a mean Mg/O-ratio of 2.14 was obtained by averaging over all the 129 experiments. This result indicates an oxygen-deficient MgO layer (cf. Ref. [36]). A changing composition during oxidation, was only observed for experiments at very low oxygen exposures (below 2 Langmuir). At higher exposures, a constant composition was observed for each single oxidation series. An oxide composition changing with oxide thickness has been found also in Ref. [74]: the composition approached a saturation value for oxide-layers ~ 5 nm thick that indicates a clear oxygen deficiency.

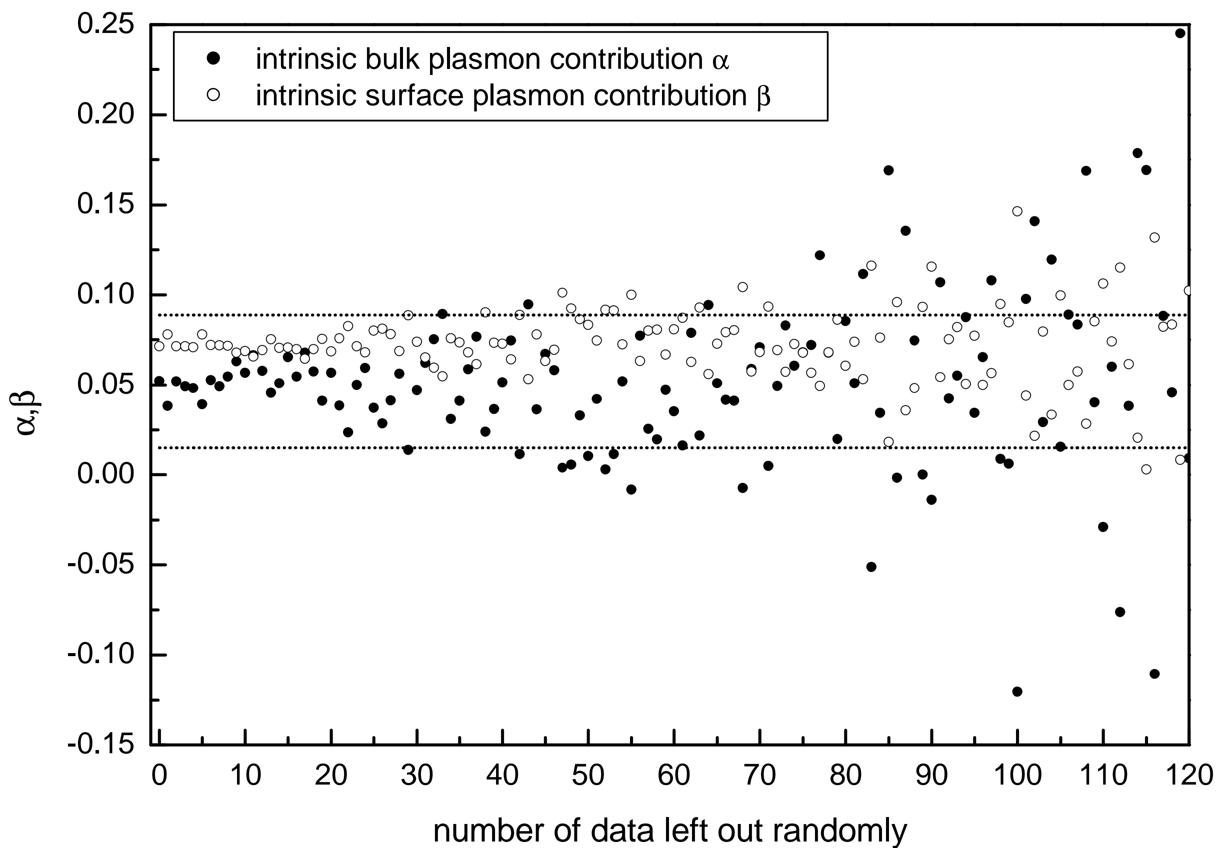

Figure 3.11: Results for α and β from evaluations of a (J_m^{ref} / J_m , J_{ox} / J_m) data set for decreasing amount of data. The (J_m^{ref} / J_m , J_{ox} / J_m) data left out were chosen randomly from the complete data set. The dotted lines represent the error limits for the α value corresponding to the complete data set.

One of the basic assumptions of the theory underlying both methods considered here is the complete disappearance of the surface plasmon contribution for the substrate after coverage with more than one monolayer of oxygen (Eq. (3.2)). This disappearance of the surface plasmon contribution, which would indicate that the initial oxide-layer is closed indeed and that thus no clean metal surface is existent any more, was verified. A series of spectra obtained for increasing oxygen exposures is shown in Fig. 3.12. It follows that the

surface plasmon contribution vanishes between an oxygen exposure of 1.0 Langmuir to 2.0 Langmuir (1 Langmuir = 10^{-6} Torr·s), which corresponds to an oxide layer-thickness of about 0.4 nm to 0.7 nm. Thus, only oxide layers with a thickness larger than 0.7 nm should be considered for the determination of α and β. Simultaneously with the decrease of the surface plasmon peak another peak builds up (Fig. 3.12), which is located at a binding energy about 5 eV larger than the main peak. The origin of this peak is not clear. This new peak has been observed by other authors, too [20,22,36,81,82]. It has been ascribed for example to an 'oxidised' surface plasmon occurring when the diameter of oxide islands from chemisorbed oxygen overcomes a critical size [20], or it may be due to an interface plasmon [22].

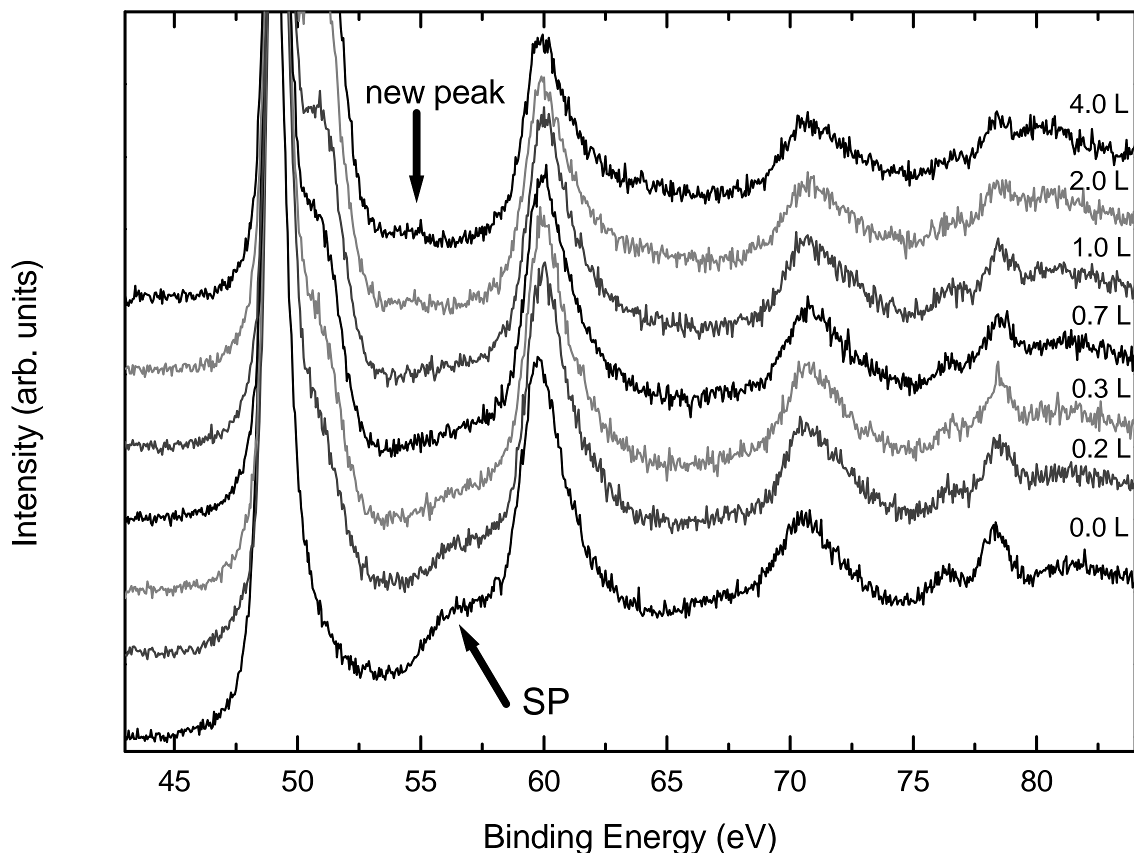

Figure 3.12: Development of the surface plasmon (SP) peak of the Mg 2p spectrum with increasing oxygen exposure from 0 L to 4.0 L corresponding to overall oxide layer thicknesses of 0 nm to 0.9 nm. The arrows indicate the position of the surface plasmon peak and the new peak emerging at about 5 eV from the main peak. The plot shows data corresponding to oxidation experiments at T = 436 K and $p_{O2} = 1.3 \cdot 10^{-7}$ Pa.

Thus, i) the presence of clean metal surface below an overall oxide-layer thickness of 0.7 nm, in combination with ii) a possible intrinsic contribution to the new loss peak and iii) possible intrinsic loss effects in magnesium oxide all might result in an underestimation of the intrinsic contribution and in changing values for α and β (see Fig. 3.8a,b and, less

pronouncedly, in Fig. 3.9a,b) because all 3 effects would be influenced by the proceeding of oxidation.

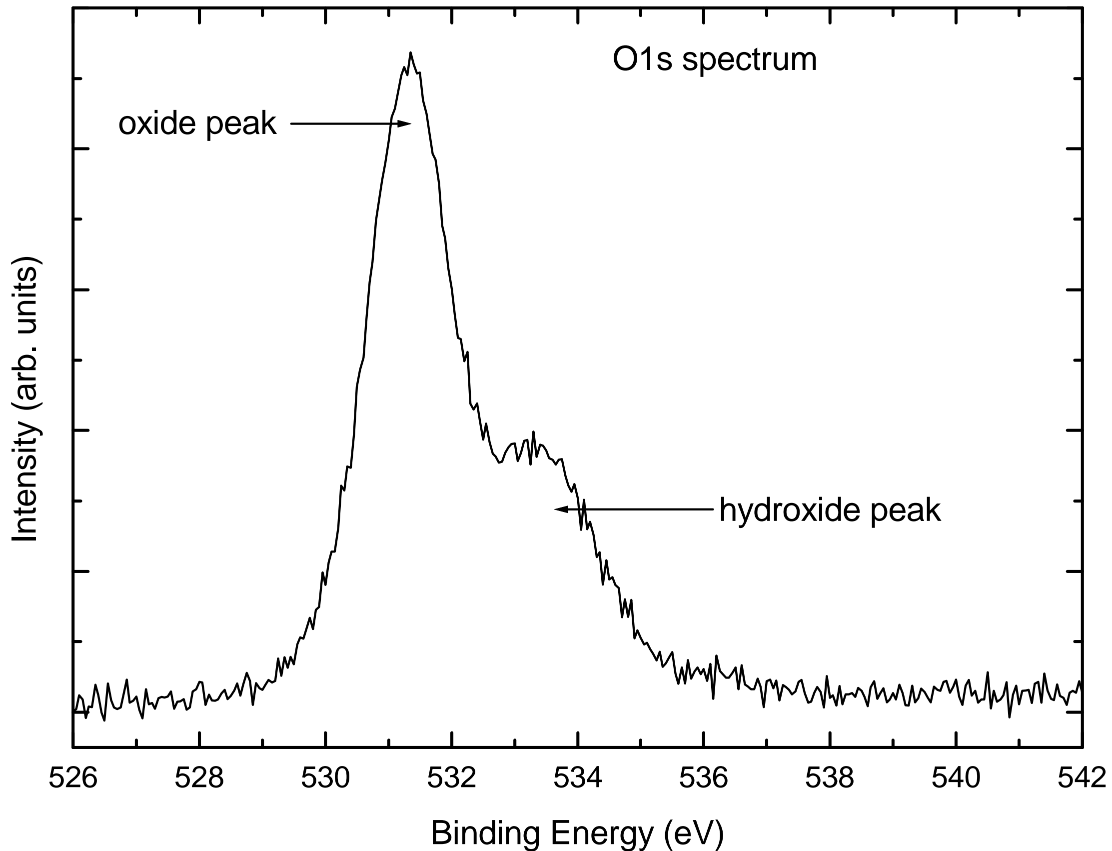

Figure 3.13: O 1s spectrum of a sample oxidised at T = 302 K and $p_{O2} = 1.3\cdot10^{-5}$ Pa for 15 min, showing a peak due to O^{2-} (low binding energy side) and due to OH^- (high binding energy side). Oxidation at lower oxygen partial pressures shows a less pronounced hydroxide peak.

For both methods (Eq. (3.8) vs. Eqs. (3.10) and (3.11)) a band gap energy of 7.8 eV, corresponding to bulk MgO (see Ref. [83]), was used in the calculation of the IMFPs, which influences the values of the constant K, α and β, the oxide thickness d_{ox} and the oxide composition of the Mg oxide present on the substrate. The thin oxide-layers considered are not stoichiometric MgO and may show a band gap value that might be lower than for bulk MgO. In Ref. [46] lower band gaps for very thin oxide layers have been suggested. To determine the effect of the band gap value on the results the evaluation procedure has been repeated for band gap values smaller than the theoretical bulk value. The results for the extreme assumption of 0 eV are $\alpha = 0.1200$ and $\beta = 0.0760$, ($\alpha + \beta = 0.1960$), for the method based on Eq. (3.8) and $\alpha = 0.1711$ and $\beta = 0.0638$, ($\alpha + \beta = 0.2349$), for the new method based on Eqs. (3.10) and (3.11). The resulting values for α and β when leaving out successively data below an increasing threshold value for oxide thickness (as in Figs. 3.8 and 3.9) are shown in Fig. 3.10 for the new method. These results are closer to the values reported

in Refs. [53,55,80], which may suggest that the band gap of very thin magnesium oxide films may be closer to 0 eV than close to the value for bulk MgO (see also Ref. [74]). This was confirmed by measurements of the extinction coefficient from ellipsometry on equally prepared and oxidised specimen (see Ref. [74]).

The O 1s spectra consist of two peaks, one peak at about 531 eV, which is assumed to originate from O^{2-} ions, and another peak at about 533 eV, which is assumed to originate from OH^- ions (Fig. 3.13; see also Refs. [16,25,28]). The intensity of this second hydroxide peak, relative to the intensity of the first oxide peak, is not constant. This might be due to a changing water content in the residual gas, depending on the particular oxidation parameters applied. After oxidation at oxygen partial pressures of $1.3 \cdot 10^{-7}$ Pa and $1.3 \cdot 10^{-6}$ Pa, the hydroxide peak is very weak and leads only to an asymmetry of the O 1s spectrum; it becomes significant upon oxidation at $1.3 \cdot 10^{-5}$ Pa.

3.6. Conclusions

(1) Two methods for separate determination of the intrinsic bulk plasmon excitation (α) and the intrinsic surface plasmon excitation (β) for free electron like metals have been evaluated critically:

i. the method based on Eq. (3.8), proposed already in Ref. [56];

ii. the method based on Eqs. (3.10) and (3.11), proposed here.

(2) Application of both methods to Mg 2p XPS spectra of pure and series of oxidised Mg showed that the method based on Eq. (3.8) is extremely sensitive to deviations in experimental data; no unequivocal results for α and β, separately, and for ($\alpha + \beta$) were obtained with this method. The alternative method yields more reliable results for α and β, separately, and for ($\alpha + \beta$). Also, the values obtained for α and β according to the alternative method are closer to experimental and theoretical data reported in literature.

(3) A useful way to asses the error magnitude and error sensitivity is to plot the results for α and β and for ($\alpha + \beta$), as a function of a limiting oxide-layer thickness value beneath which data have been left out of the analysis.

(4) The deviations from constancy observed for α and β, and for ($\alpha + \beta$) in the above mentioned plots have been shown for the case considered, at least partly, to be of systematic nature. The following systematic error sources have been identified:

i. The surface plasmon peak from the metal substrate is visible up to a value of about 0.7 nm oxide thickness. Thus, below this apparent thickness value the oxide layer is not closed. Above this thickness value the layer has an inhomogeneous thickness.

ii. Together with the disappearance of the surface plasmon peak, due to coverage of the metal surface with oxygen, a new peak appears at a distance of about 5 eV from the main peak.

iii. The composition of the oxide layer does not correspond to MgO. Probably a varying hydroxide contribution is present in the oxide layer, depending on the temperature and oxygen partial pressure applied.

iv. The use of a band gap energy value smaller than the theoretical one for bulk MgO for the calculation of the IMFP in the oxide, yields more reasonable results (see (2) above) for both methods. The assumption of a band gap of 0 eV yielded with the alternative method values of $\alpha = 0.17$ and $\beta = 0.06$.